A Model of Action Potentials and Fast Ca^{2+} Dynamics in Pancreatic β-Cells

L. E. Fridlyand,* D. A. Jacobson, A. Kuznetsov, and L. H. Philipson
Department of Medicine, University of Chicago, Chicago, Illinois

ABSTRACT We examined the ionic mechanisms mediating depolarization-induced spike activity in pancreatic β-cells. We formulated a Hodgkin-Huxley-type ionic model for the action potential (AP) in these cells based on voltage- and current-clamp results together with measurements of Ca^{2+} dynamics in wild-type and Kv2.1 null mouse islets. The model contains an L-type Ca^{2+} current, a "rapid" delayed-rectifier K^+ current, a small slowly-activated K^+ current, a Ca^{2+}-activated K^+ current, an ATP-sensitive K^+ current, a plasma membrane calcium-pump current and a Na^+ background current. This model, coupled with an equation describing intracellular Ca^{2+} homeostasis, replicates β-cell AP and Ca^{2+} changes during one glucose-induced spontaneous spike, the effects of blocking K^+ currents with different inhibitors, and specific complex spike in mouse islets lacking Kv2.1 channels. The currents with voltage-independent gating variables can also be responsible for burst behavior. Original features of this model include new equations for L-type Ca^{2+} current, assessment of the role of rapid delayed-rectifier K^+ current, and Ca^{2+}-activated K^+ currents, demonstrating the important roles of the Ca^{2+}-pump and background currents in the APs and bursts. This model provides acceptable fits to voltage-clamp, AP, and Ca^{2+} concentration data based on in silico analysis.

INTRODUCTION

Excitable cells express voltage-gated Ca^{2+} channels (VGCCs) along with K^+ channels that precisely regulate action-potential (AP) firing, triggering a variety of biochemical events involved in the control of cell function. In general, the profile of the AP waveform and the gating properties of the VGCCs determine the peak and duration of the voltage-gated Ca^{2+} current (I_{VCa}), which in turn dictates the pattern of Ca^{2+} influx. Changes in the AP profile can alter AP-driven Ca^{2+} signaling. This is of physiological relevance especially for pancreatic β-cells, in which Ca^{2+} dynamics are accompanied by changes in insulin secretion (1–3).

Over the physiological range of glucose concentrations, β-cell electrical activity often consists of depolarizing bursts in plasma membrane potential (V_m). These occur as depolarized plateaus, on which the bursts of APs occur separated by repolarized electrically silent intervals. Riding on these depolarized plateaus, the rapid voltage spikes (frequency, 1–5/s), which further depolarize the electrical syncitium of islet β-cells to ~−20 mV. Bursts become continuous spikes at high glucose levels (4–8). Spike and burst behavior depend on multiple different channels, modified by inhibitors and activators as well as by posttranslational modification and changes in gene expression. The pattern of electrical activity likely involves complex interactions between many different ion channels (1,2). However, the mechanisms underlying spikes and burst behavior in pancreatic β-cells have been incompletely characterized.

In this study, we examined the ionic mechanisms mediating depolarization-induced spike activity using electrophysiological experiments, Ca^{2+} measurements with high temporal resolution, and a novel computational model based on the properties of individual β-cell currents. We simulated the experimental data obtained for mouse islets, because they have been the most thoroughly studied. Although several ionic models for β-cell spikes have been described (9–12), they include a limited subset of channels. Experimental data obtained with recently characterized channel modifiers and, in particular, data on the Kv2.1$^{-/-}$ mouse model indicate that a broader set of channels and pumps are involved in regulating insulin secretion. Here, we describe a more extensive model to consider an extended variety of ion channels and we show how this model can be used to investigate spontaneous V_m activity, initiation and termination of the bursts of spikes, and Ca^{2+} dynamics in pancreatic β-cells.

METHODS AND THEORY

V_m recordings and calcium measurements

To test the role of K^+ channels in glucose-stimulated APs, intact mouse islet β-cell membrane potentials were recorded using the perforated-patch current-clamp configuration. Ca^{2+} measurements were also made with high temporal resolution. Experimental methods were performed as previously described (13–15).

Formulation of the model

To provide a rigorous quantitative test of the experimental data, we developed a mathematical model in which specific ionic currents were included (Fig. 1). The differential equation describing time-dependent changes in the plasma membrane potential is the current balance equation:

$$-C_m\frac{dV_m}{dt} = I_{VCa} + I_{KDr} + I_{KVs} + I_{KATP} + I_{KCa} + I_{Cap} + I_{Nab}, \quad (1)$$

where I_{KDr} is the rapid delayed-rectifier current, I_{KVs} is the slowly-activated K^+ current, I_{KATP} is the ATP-sensitive K^+ channel current, I_{KCa} is the Ca^{2+}-activated K^+ current, I_{Cap} is the plasma membrane Ca^+-pump current, and

Submitted July 25, 2008, and accepted for publication January 16, 2009.

*Correspondence: lfridlia@medicine.bsd.uchicago.edu

Editor: Eduardo Perozo.

0006-3495/09/04/3126/14 $2.00

doi: 10.1016/j.bpj.2009.01.029

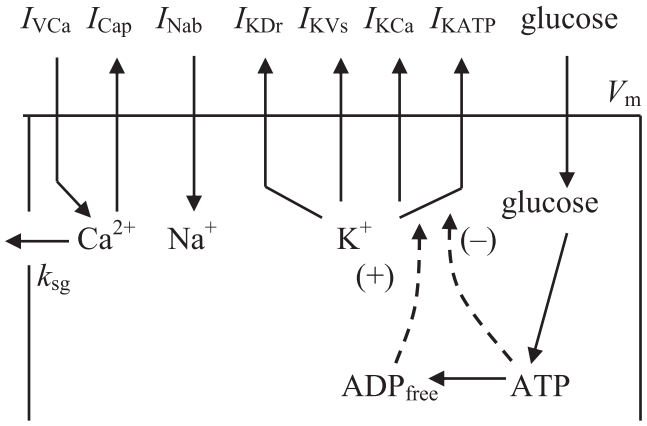

FIGURE 1 Schematic diagram of the ionic current and Ca^{2+} fluxes. Transmembrane currents are the I_{VCa}, the I_{Cap}, the I_{Nab}, the I_{KDr}, the I_{KVs}; the I_{KCa}; and the I_{KATP}. Calcium enters the β-cells primarily through voltage-activated Ca^{2+} channels by diffusion along an inwardly-directed electrochemical gradient. At the plasma membrane, two processes are involved in transporting Ca^{2+} out of the cell: a Ca^{2+} pump, and removal of Ca^{2+} sequestrated in insulin granules by exocytosis (coefficient k_{sq}).

I_{Nab} is the Na^+ background current. *C*m is the whole-cell membrane capacitance. The currents are listed in Fig. 1.

A conventional Hodgkin-Huxley-type model was used for time-dependent Ca^{2+} and K^+ channels. Boltzman-type equations are assumed for steady-state activation and inactivation functions (Appendix). The gating variables were set equal to their steady-state values, if the time constants of the activation and/or inactivation of the gating variables are small in comparison with the time interval for one spike. Coefficients used in this model were either adopted from the model of Fridlyand et al. (16,17) or are described here. The parameters for which there are no specific experimental data were chosen to be consistent with experimental data presented here, as well as previously published data, to obtain the proper magnitude of the voltage and frequency of the spikes that were experimentally recorded in β-cells. However, all parameters and constants were fitted to be in their physiological ranges. A full set of current equations and parameter values are given in the Appendix and Tables 1 and 2.

Voltage-gated Ca^{2+} current (I_{VCa})

The whole-cell Ca^{2+} current in mouse β-cells flows principally through VGCCs (2,18,19). In addition to having superior conductance properties, Ca^{2+} channels undergo rapid but incomplete inactivation during sustained depolarizing voltage pulses (20,21). β-cells also display a slow Ca^{2+}-dependent inactivation (19,22–24). Modeling the inactivation behavior of Ca^{2+} channels involves both voltage and calcium dependence, and several models have been proposed to reproduce this behavior (25–27). In our case, we used the activating gating variable (d_{Ca}) (Eq. A2) and two inactivating gating variables: one rapid and voltage-sensitive (f_{VCa}) and the other slow and Ca^{2+}-dependent (f_{2Ca}). Our introduction of these two inactivating gating variables for a Hodgkin-Huxley-type model of Ca^{2+} current is based on discussions by others (25,26).

The steady-state activation curve ($d_{Ca\infty}$) (Eq. A3) can be described by a Boltzman-type equation (28,29). Ca^{2+} channels open rapidly upon membrane depolarization, with a time constant of ~1 ms (24,27), and we obtained the equation for the activation time (τ_{dCa}) (Eq. A4) by fitting data from Fig. 4 *B* of Gopel et al. (24).

We used the conventional equation for voltage-sensitive inactivating gating variables (f_{VCa}) (Eq. A5). Ca^{2+} channels close rapidly after a depolarizing pulse (28), and we suggest that the time for f_{VCa} inactivation is also very fast, e.g., $f_{VCa} = f_{VCa\infty}$. The steady-state inactivation curve for $f_{VCa\infty}$ (Eq. A5) was adopted as a Boltzman-type equation.

TABLE 1 Cell and membrane current parameters

Parameter	Definition	Value	Reference
C_m	Membrane capacitance	6158 pF	16
V_i	Cytosol volume	0.764 pL	16
f_i	Fraction of free Ca^{2+} in cytoplasm	0.01	16
F	Faraday constant	96,487.0 C/mol	
k_{sg}	Coefficient of the sequestration rate of $[Ca^{2+}]_i$.	0.0001 ms^{-1}	16
g_{mVCa}	Maximum conductance for I_{VCa}	1500 pS	*f*
g_{mKDr}	Maximum conductance for I_{KDr}	45,000 pS	*f*
g_{mKVs}	Maximum conductance for I_{KVs}	2200 pS	*f*
g_{mKCa}	Maximum conductance for I_{KCa}	20 pS	*f*
g_{mNab}	Maximum conductance for I_{Nab}	25 pS	*f*
g_{mKATP}	Maximum conductance for I_{KATP}	30,000 pS	*f*
P_{mCap}	Maximum I_{Cap} current	4800 fA	*f*
K_{KCa}	Half-maximum Ca^{2+} binding constant for I_{KCa}	0.1 μM	16
K_{Cap}	Half-maximum Ca^{2+} binding constant for I_{Cap}	0.1 μM	16
E_{Ca}	Reversal potential for Ca^{2+} current	100 mV	9
E_K	Reversal potential for K^+ current	−75 mV	16
E_{Na}	Reversal potential for Na^+ current	70 mV	26
τ_{dKDr}	Time constant for d_{KDr}	25 ms	*f*
τ_{dKs}	Time constant for d_{Ks}	300 ms	*f*

f, adjusted to fit the experimental values.

We formulated a new equation for the slow Ca^{2+}-dependent inactivating gating variable (f_{2Ca}), because cytoplasmic Ca^{2+} changes during one spike apparently do not exceed 0.1 μM over the basal level in pancreatic β-cells, leading to only insignificant changes in f_{2Ca} if we used the coefficients represented in other models (25,26) for cardiac muscle cells. The dynamics of Ca^{2+} channels seem similar to the predominant L-type channel, but they have not been investigated in sufficient detail in pancreatic β-cells to completely understand differences in the kinetics of inactivation. However, Shermann et al. (30) suggested that Ca^{2+}-current-dependent inactivation of I_{VCa} better reflects the inactivation process in β-cells over a simple Ca^{2+}-concentration-dependent inactivation. Therefore, we have suggested that the rate of inactivation of f_{2Ca} is proportional to a Ca^{2+} current through a unitary channel (the term I_{VCa}/g_{mVCa} in Eq. A6) rather than Ca^{2+} concentration as has been suggested in other models (25,26). The dynamic of f_{2Ca} is determined by the relative rates of activation and inactivation (Eq. A6). Parameters (Table 1) were set so that the difference in the magnitude of I_{VCa} was most pronounced at potentials from −45 to −10 mV, in the characteristic functional range of mouse β-cells (19,24,29).

We simulated the double-pulse protocol for voltage-clamp measurements to compare the predictions of the model with specific experiments (Fig. 2 *A*). The f_{2Ca} variable undergoes an I_{VCa}-dependent inactivation. Time dependence of Ca^{2+} currents and an initial inactivation time (~20 ms) are in good quantitative agreement with experimental data (19,22,24,29). Simulated voltage dependence of whole-cell peak calcium currents are shown in Fig. 2 *B*. The simulated peak I/V curve also compares well with experimental results (19,24,28,29).

Rapid delayed-rectifier K^+ current (I_{KDr})

Voltage-gated K^+ channels (K_v) determine AP repolarization in the pancreatic β-cells. The principal voltage-gated K^+ current in mouse β-cells, a relatively rapid delayed-rectifier K^+ current (I_{KDr}), is responsible for >80% of the current (2,13,24,31–33).

A Hodgkin-Huxley-type model for I_{KDr} with activation (d_{KDr}) and inactivation (f_{KDr}) gating variables was used (see Appendix Eqs. A7 and A8).

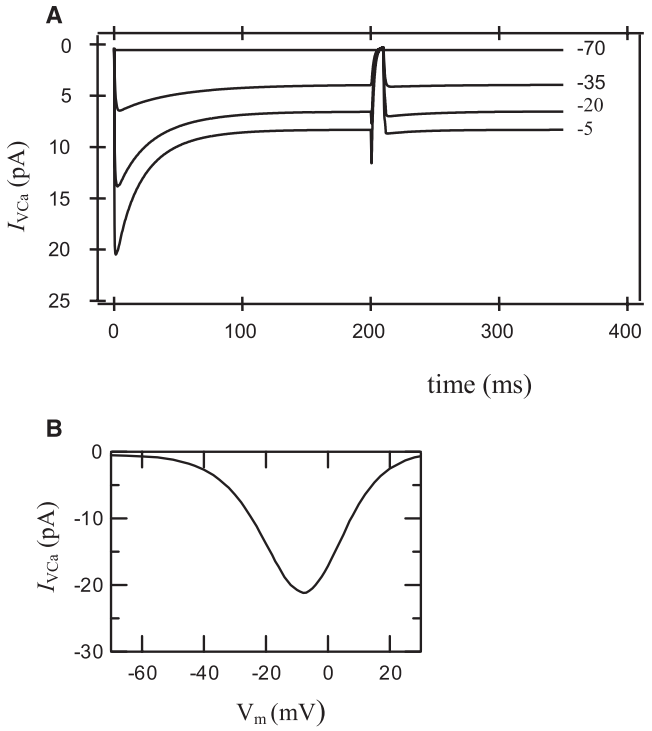

FIGURE 2 (*A*) Simulation of voltage-clamp experiments for a Ca^{2+} current (I_{VCa}), using a double-pulse protocol. The membrane potential was stepped from the holding potential (−70 mV), where $d_{Ca} = 0.00244$ and $f_{2Ca} = 0.884$, to the prepulse potential (pointed in figure) for 200 ms. Voltage was then stepped back to the holding potential (−70 mV) for 10 ms and finally stepped to test potential. Current record simulations were made for prepulses (−70, −35, −20, −5 mV). (*B*) Simulated voltage dependence of whole-cell peak calcium currents obtained as in the left part of Fig. 2 *A*. Current parameters and equations for I_{VCa} are shown in Table 1 and the Appendix.

Inactivation of I_{KDr} was negligible during a 200-ms depolarization (14,24,31). Therefore, we have suggested that $f_{KDr} = 1$. The activation of the I_{KDr} could be described by n^2 kinetics (31). Activation time for d_{KDr} (τ_{dKDr}) is in the range of 10–30 ms (14,24,28) and was approximated as a constant (Table 1), chosen to provide an acceptable frequency of glucose-induced spikes that corresponds to experimental data. The value of g_{mKDr} (Eq. A7) was calculated as 45 nS for standard conditions (Table 1).

Slow-activated TEA-insensitive K^+ current

A minor part of the K_V current in insulin-secreting cells from mouse islets or β-cell lines is insensitive to tetraethylammonium ion (TEA), a nonspecific pharmacological blocker of voltage-gated K^+ channels ((34–37), see also Discussion). Therefore, we now include a TEA-insensitive small-conductance slow-voltage-activated K^+ current (I_{KVs}) regulating the TEA-induced AP duration and frequency. For simplicity, we propose that maximum conductance of this current is 10% of the maximum conductance for I_{KDr} (Table 1), in agreement with experimental evidence that this current is small. For simplification, we also set its voltage-gated characteristics similar to those of I_{KDr} (Eqs. A10–A12), except that its activation time constant (τ_{dKs}) (300 ms for I_{KVs}) is considerably longer than for I_{KDr}.

Currents with time- and voltage-independent gating variables during one spike

To isolate the rhythmogenic potential of the currents considered above, we have also included several additional currents with gating variables that are time- and voltage-independent during one spike interval. They serve as background currents and can be modeled without using activation and inactivation voltage-dependent gating variables.

ATP-sensitive K^+ current

K_{ATP} channels are the predominant inwardly rectifying potassium channel β-cells. They maintain the resting potential in quiescent β-cells at ~−70 mV, slightly elevated from the electrochemical equilibrium potential for K^+ (~−75 mV). Free ATP inhibits K_{ATP} channels, whereas intracellular free ADP ($[ADP]_i$) activates them. Glucose elevates the intracellular concentration ratio of ATP to ADP that causes K_{ATP} channel closure and membrane depolarization (1,17). The endogenous K_{ATP} current is reasonably linear over the physiological voltage range (38,39). This current can be simulated by a term relating dependence of K^+ flux to resting potential, i.e., $V - E_K$ (10,11,40). We adopted a kinetic model (Eqs. A13–A15 in the Appendix) for the value of whole-cell K_{ATP} channel conductance from Fridyland et al. (17). Maximum conductance for I_{KATP} is close to that employed previously (17) and falls in the range that was measured for the maximum K_{ATP} conductance for β-cells.

Ca^{2+}-activated K^+ currents with time- and voltage-independent gating variables

Different Ca^{2+}-activated K^+ (K_{Ca}) channels with time- and voltage-independent gating variables are expressed in β-cells. (Eqs. A16 and A17). These include both TEA-sensitive K_{Ca} channels (31,33,35) and channels that have lower sensitivity to TEA (33,41,42). We included a calcium-activated K^+ current as the current termed I_{KCa} from our model (16).

Plasmalemma Ca^{2+}-pump current

Plasma membrane Ca^{2+} pumps are capable of establishing a membrane potential when operating with $H^+/Ca^{2+} = 1$ (43). For this reason, Ca^{2+} pumps provide an outward current (I_{Cap}) and also contribute to V_m (Eq. A18). The equation, the maximum rate, and the half-maximum Ca^{2+}-binding constant for I_{Cap} were adapted from Fridlyand et al. (16).

Na^+ background current

A tetrodotoxin-insensitive Na^+ inward current has been described in β-cells. It may be an Na^+ current through nonselective cation channels with time- and voltage-independent gating variables (16,44–47). This current can be considerable, because there is a large difference in Na^+ concentration between the cytoplasm and the surrounding medium. We have included this current (I_{Nab}) in our model as a linear Na^+ background current. We used the equation for I_{Nab} (Eq. A19) according to the model of Luo and Rudy (26).

Currents not included in the model

Application of tetrodotoxin, a specific voltage-gated Na^+ channel blocker, is known to have a negligible effect on APs in mouse β-cells (1,24). The picture in human cells is more complex for the inward current (33,48,49), but as we are focusing on the mouse, we did not include a Na^+ voltage-dependent current in this model.

The Na^+-K^+ pump extrudes three Na^+ ions from the cell in exchange for two K^+ ions, generating a net outward current. Currents provided by Na^+-Ca^{2+} exchangers also contribute to V_m. Both these currents were included in our recent β-cell ionic model (16,17). Other inward and outward currents have also been found in β-cells (1,2,16). The changes in their conductance do not appear to play a role in the short time interval during one spike, so we do not consider these currents in our model. We have included in our model the time- and voltage-gated independent outward (I_{KCa}, I_{Cap}, and I_{KATP}) as well as inward (I_{Nab}) currents and suggest that a combination of these currents is sufficient to describe the effects of the background currents during one spike interval.

TABLE 2 Initial conditions for state variables at low glucose level

Variable	Definition	Initial value
V_m	Membrane potential	−59.4 mV
d_{Ca}	I_{VCa} activation gating variable	0.00346
f_{2Ca}	I_{VCa} slow-inactivation gating variable	0.856
d_{KDr}	I_{KDr} activation gating variable	$4.17\ 10^{-5}$
d_{Ks}	I_{KVs} slow-activation gating variable	$4.17\ 10^{-5}$
$[Ca^{2+}]_i$	Intracellular Ca^{2+} concentration	0.08 μM

Unless otherwise noted, $[ADP]_i = 100\ \mu M$.

Ca^{2+} dynamics

Based on the considerations in our general model (16), and including only I_{VCa} and I_{Cap}, the equations for free cytoplasmic Ca^{2+} ($[Ca^{2+}]_i$) dynamics can be written as

$$\frac{d[Ca^{2+}]_i}{dt} = \frac{f_i(-I_{VCa}-2I_{Cap})}{2FV_i} - k_{sg}[Ca^{2+}]_i, \qquad (2)$$

where f_i is the fraction of free Ca^{2+} in cytoplasm, F is Faraday's constant, V_i is the effective volume of the cytosolic compartment, and k_{sg} is a coefficient of the sequestration rate of $[Ca^{2+}]_i$.

Simulation methods

The complete system consists of six state variables: differential equations describing the time rate of change in membrane voltage (V_m) (Eq. 1), $[Ca^{2+}]_i$ (Eq. 2) and voltage-dependent gating variables d_{Ca} (Eq. A2), f_{2Ca} (Eq. A6), d_{KDr} (Eq. A8), and d_{Ks} (Eq. A11).

Equations and parameter values (Table 1) and initial conditions (Table 2) contain all the information necessary to carry out the simulations presented in this article. The parameters (units) are time (ms), voltage (mV), concentration (μM), current (fA), conductance (pS), and capacitance (fF). Numerical integration of the Hodgkin-Huxley-type ionic model was carried out using standard numerical methods (16,17). This model is available for direct simulation on the website "Virtual Cell" (www.nrcam.uchc.edu) in "Math-Model Database" on the "math workspace" in the library "Fridlyand" with name "MouseSpike". Visualization and graphical analysis were performed using Igor Pro (WaveMetrics, Lake Oswego, OR).

RESULTS

AP and Ca^{2+} measurements

Fig. 3 *A1* shows typical glucose-induced single-spike behaviors on depolarized plateaus of bursts for wild-type mouse islets. Our studies with wild-type mouse islets showed also that Kv2.1 inhibition with stromatoxin increases the amplitude of glucose-induced APs but decreases their frequency while increasing their width (14). A typically complex structure of one spike after stromatoxin action with several V_m oscillations is shown in Fig. 3 *A2*. Application of TEA in the mouse β-cell prolongs the AP duration and increases its amplitude (Fig. 3 *A3*). Loss of Kv2.1 in the Kv2.1 null mouse (Fig. 3 *B*) caused glucose-stimulated AP duration to increase, with an associated reduction in AP firing frequency and a new complex AP structure that resembled the effects of specific Kv2.1 inhibitors (compare Fig. 3, *A2* and *B1*). On the other hand, TEA has effects in Kv2.1 null islets similar to those in control wild-type islets (compare Fig. 3, *A3* and *B2*). Every glucose-induced AP is accompanied by

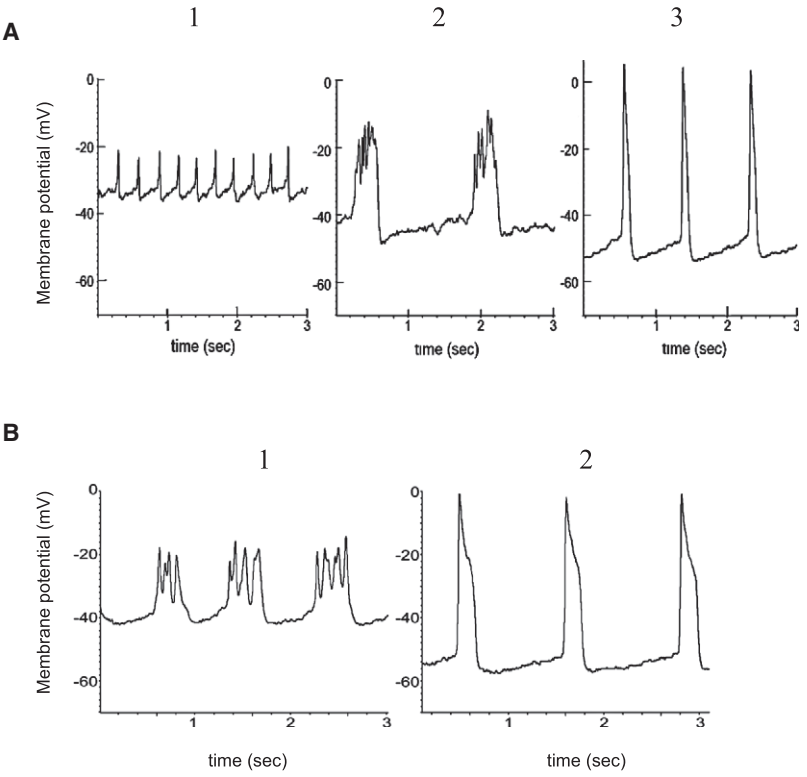

FIGURE 3 (*A*) Control islets from wild-type mouse treated with stromatoxin and TEA. Control islet electrical activity was recorded during treatment of 14 mM glucose alone (*1*), or in combination with 100 nM stromatoxin ScTx-1 (*2*) or 15 mM TEA (*3*). Representative APs are shown. (*B*) Kv2.1$^{-/-}$ islet electrical activity in response to 14 mM glucose (*1*) or in combination with 15 mM TEA (*2*). Representative APs are shown.

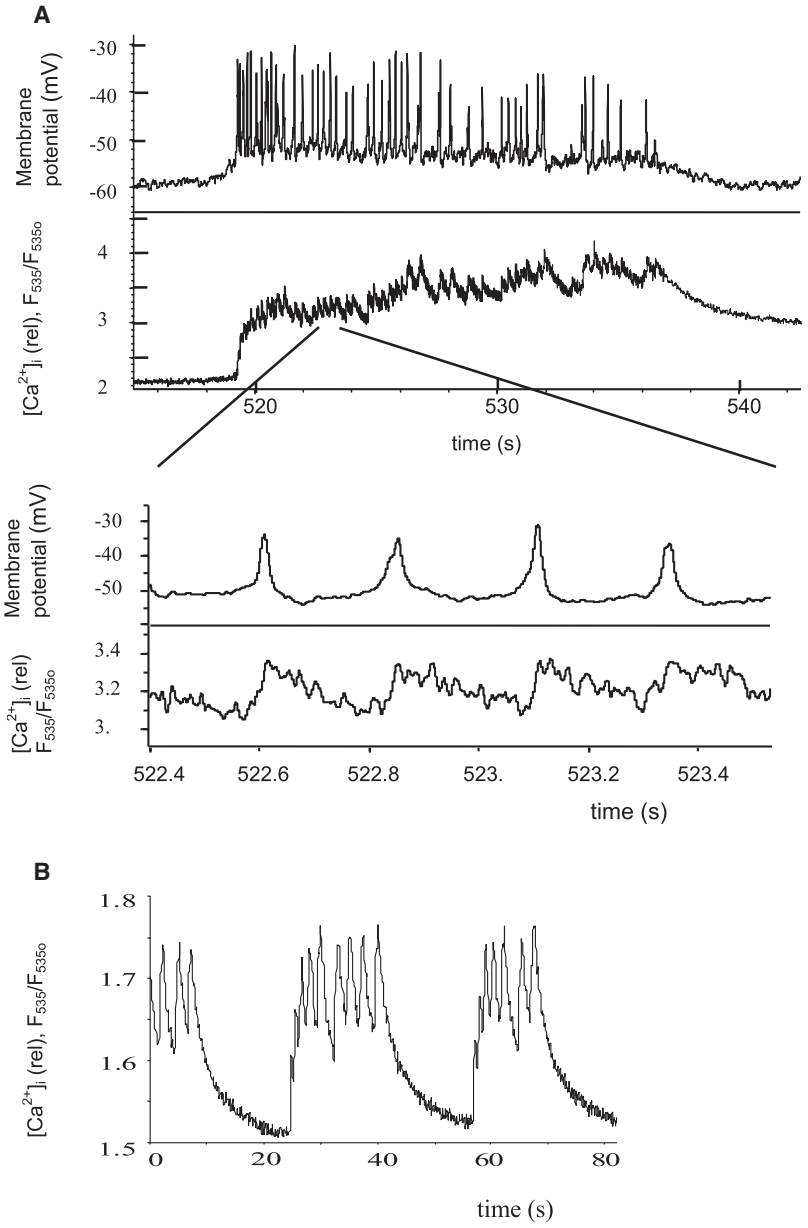

FIGURE 4 Experiments with relative Ca^{2+} measurement (as F_{535}/F_{535o} (13–15)). (*A*) Glucose-induced bursts and spikes with simultaneous APs and Ca^{2+} measurement in control islets from wild-type mouse during treatment with 14 mM glucose. The lower record represents, at a faster timescale, part of the upper record. (*B*) TEA-induced bursts and Ca^{2+} spikes in control mouse islet at 14 mM glucose and 20 mM TEA.

a $[Ca^{2+}]_i$ spike (Fig. 4 *A*, showing one burst). Measurements of relative Ca^{2+} changes after application of TEA during several bursts are shown in Fig. 4 *B*. In this case, relative $[Ca^{2+}]_i$ changes during one spike were significantly higher after TEA application than during glucose-induced spikes in Fig. 4 *A*. Note that we performed only relative Ca^{2+} measurements. For this reason, we compared a relative change of Ca^{2+} level during one spike with the relative Ca^{2+} level during the repolarized electrically silent interval between bursts to make a valid comparison among different experiments. Relative Ca^{2+} changes during one glucose-induced spike in Kv2.1 knockout mouse islets that were measured by Jacobson et al. (14) also had greater relative amplitude compared with wild-type islets.

Modeling of spikes and generation of bursts in pancreatic β-cells

Spontaneous glucose-induced spike activity in wild-type β-cells

In our model, the membrane potential reaches the AP threshold through the depolarizing effect of decreased I_{KATP}. Increased glucose was modeled by closure of K_{ATP} channels after a rise in [ATP]/[ADP] (6,17). The resting membrane potential was –59.4 mV at 100 μM free $[ADP]_i$ (Table 2). K_{ATP} channel closure was simulated by a decrease of $[ADP]_i$ from 100 μM to 15 μM, leading to depolarization and spontaneous spiking (Fig. 5 *A*, *arrow 1*). The result gives the continuous spike activity in this simulation, as in Fig. 6 *A*.

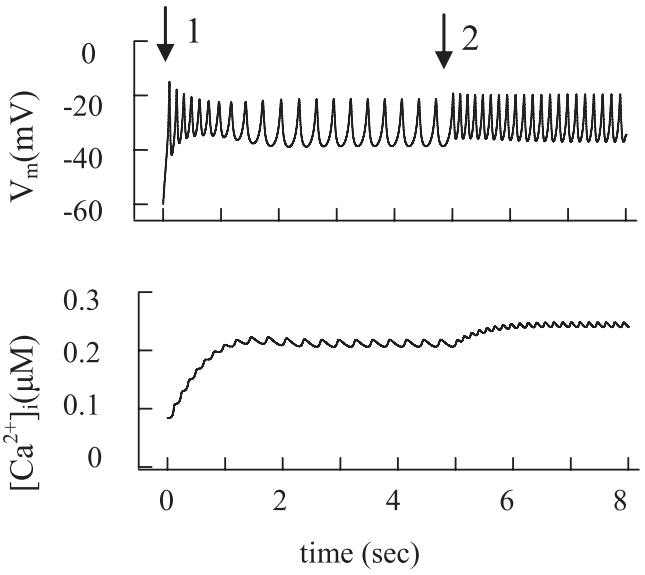

FIGURE 5 Modeling of spontaneous glucose-stimulated spikes and changes of the intracellular Ca^{2+} concentration. Glucose-induced spikes were simulated at a step decrease of the free $[ADP]_i$ at arrow 1 from a high to an intermediate value (from 100 μM to 15 μM) at $t = 0$ and at initial parameters as in Table 2; all other parameter settings are standard (Table 1). To simulate a glucose increase, the free $[ADP]_i$ was decreased from 15 μM to 8 μM at arrow 2. (*B*) Corresponding changes in $[Ca^{2+}]_i$ were simulated using Eq. 2.

The simulated closing of additional K_{ATP} channels after an initial glucose-induced depolarization was simulated by a reduction in free [ADP] (Fig. 5 *A*, *arrow 2*) that leads to decreased K_{ATP} channel conductance in our model (resulting V_m depolarization and $[Ca^{2+}]_i$ changes are shown in Fig. 5). The simulated AP agrees with a large body of experimental data (Fig. 3 *A1* and Fig. 4 *A*) (2,4,5,7,8,14,28,33).

The possible mechanisms underlying the AP, $[Ca^{2+}]_i$ changes, and roles of different currents can be better understood by considering the voltage-dependent currents during one spike (Fig. 7). Fig. 7 *A* shows V_m, $[Ca^{2+}]_i$, and the various currents during a simulation of one spike of a glucose-generated AP, as in Fig. 6 *A*. In agreement with the suggestion of Rorsman and Trube (28), the depolarizing phase of the action potential results from activation of voltage-gated Ca^{2+} channels. Activation of rapid delayed-rectifier K^+ channels (current I_{KDr}) is responsible for a repolarization of the AP. I_{KVs} contributes insignificantly to depolarization, since this current is small in comparison with I_{KDr}. Other currents are small and in this model have an insignificant influence on AP.

Specific blockers of voltage-gated K^+ channels and Kv2.1 null mouse

To investigate the role of voltage-gated K^+ channels, we simulated spikes with decreasing ''rapid'' delayed-rectifier K^+ channel conductance (Figs. 6 *B* and 7 *B*), which corresponds in action to some specific blockers of voltage-gated K^+ channels, or islets from the Kv2.1 null mouse.

According to Jacobson et al. (14) Kv2.1$^{-/-}$ β cells have a current amplitude that is only 17% that of control wild-type. Pharmacological inhibition of Kv2.1 caused a similar degree of reduction in control β cells. However, only 53% of the remaining Kv current was sensitive to block by TEA (14). Consequently, the TEA-sensitive remaining Kv current amounts to ~9% of the total Kv current in control wild-type cells. In line with these data, the simulated decreased I_{KDr} conductance was only 10% of the total I_{KDr} conductivity used in the simulation of glucose-induced spikes for control wild-type in Figs. 6 *A* or 7 *A*. The overall shape of the simulated AP (Figs. 6 *B* or 7 *B*) resembles the experimental AP seen in AP studies after application of the Kv2.1 channel blocker stromatoxin (Fig. 3 *A2*) or in islets from the Kv2.1$^{-/-}$ mouse (Fig. 3 *B1*, and see Jacobson et al. (14)).

Fig. 7 *B*, shows V_m, $[Ca^{2+}]_i$, and the various currents during simulation of one spike, as in Fig. 6 *B*. The major depolarizing current for single spikes was again I_{VCa}, as in Fig. 7 *A*. The remaining part of I_{KDr} in the interaction with I_{VCa} generated several fast V_m oscillations in the plateau phase of an AP by the same mechanisms as observed at

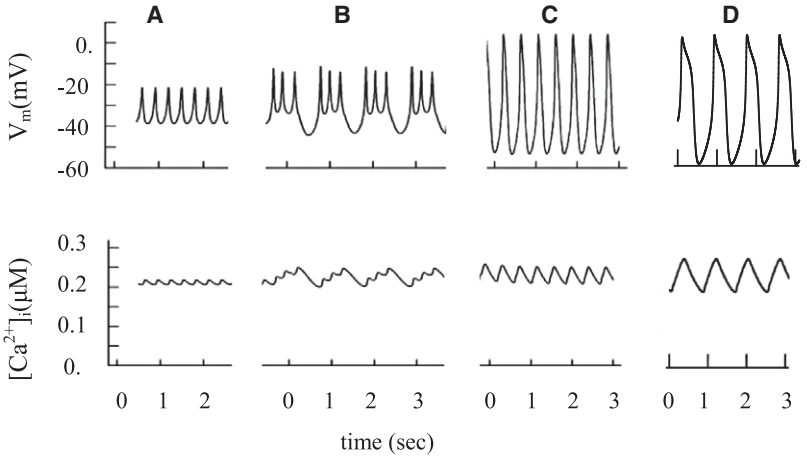

FIGURE 6 Simulated glucose-induced spike behavior and $[Ca^{2+}]_i$. of glucose-induced spikes with the same initial simulation as in the beginning of Fig. 5 (*A*) and of Kv2.1 channel blocking (*B*). For simulation of Kv2.1 channel blocking, the maximal conductance (g_{mKDr}) for the delayed rectifier K^+ channels was decreased from 45,000 pS to 4500 pS, and τ_{dKDr} was decreased from 25 ms to 20 ms. (*C* and *D*) Simulation of TEA action. In both cases, the maximal conductance for TEA-dependent K^+ channels was decreased: from 30,000 to 15,000 pS for K_{ATP} (g_{mATP}), and from 45,000 pS to 45 pS for delayed-rectifier K^+ channels (g_{mKDr}). In addition, for the mechanism in *C*, the maximal conductance for K_{Ca} channels (g_{mKCa}) was decreased from 20 pS to 0.1 pS. In the case of the mechanism in *D*, g_{mKCa} was increased from 20 to 200 pS and K_{KCa} was increased from 0.1 μM to 0.3 μM (Eq. A17). However, I_{KVs} was eliminated ($g_{mKs} = 0$).

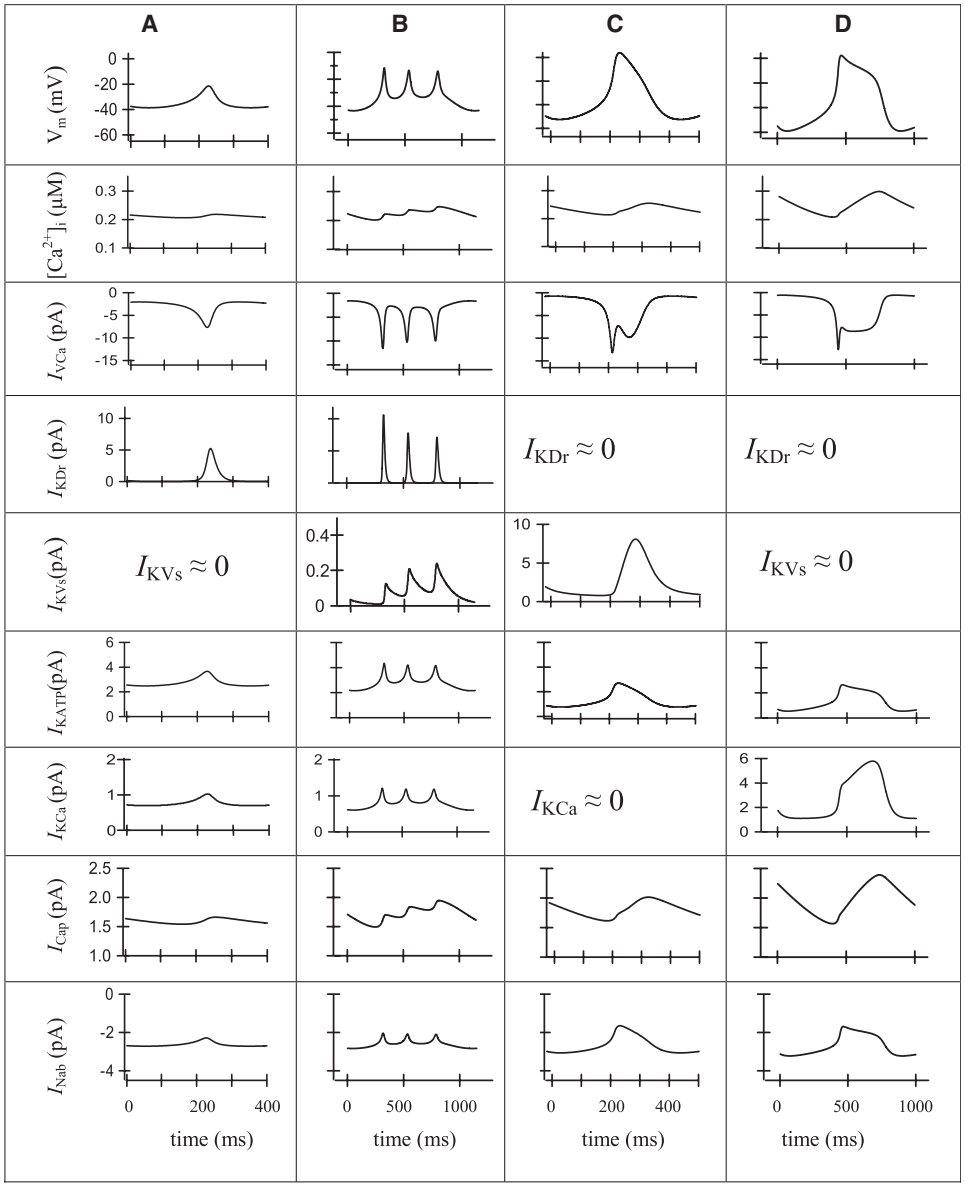

FIGURE 7 Simulation of single spikes. Action potential (V_m), $[Ca]_i$, I_{VCa}, I_{KDr}, I_{KVs}, I_{KATP} I_{KCa},, I_{Cap}, and I_{Nab} are represented for one characteristic spike. The units are shown in series, as labeled in the first column, if no units are represented on the axis. (*A*) The model solution is represented for the spike after simulation of glucose addition as in Fig. 5 or Fig. 6 *A*. The I_{KVs} and I_{KCa} currents are minor contributors in this mode of oscillation. (*B*) A single characteristic spike after simulation of Kv2.1 blocker application, as in Fig. 6 *B*. The I_{Cap} and I_{KVs} currents are the major contributors in this repolarizing part of the AP. (*C*) A single characteristic spike after simulation of TEA action as in Fig. 6 *C*. The proposal for full blocking of I_{KCa} current was accepted ($I_{KCa} \approx 0$). The I_{KVs} and I_{Cap} currents are the major contributors in this repolarizing part of the AP. (*D*) A single characteristic spike as in Fig. 6 *D* after simulation of TEA action in a model that incorporates Ca^{2+}-dependent TEA-independent K^+ channels (current I_{KCa}) instead of a slow-activated TEA-insensitive K^+ current ($I_{KVs} = 0$). In this case, $g_{mKCa} = 200$ pS, $K_{KCa} = 0.3$ μM (Eq. A17) and $g_{mKs} = 0$. The I_{KCa} and I_{Cap} currents are the major contributors in the repolarizing part of AP.

glucose-generated AP in Fig. 6 *A*. However, it occurs at higher V_m levels, where I_{KDr} has an increased value even at small conductance. During the single spike, the slow-activating TEA-insensitive K^+ channels (I_{KVs}) contribute increasingly in AP, because the time constant for their activation was evaluated in the range of several hundred milliseconds in our model. Increased I_{KVs} leads to a repolarization. However, the simulated increase of I_{KCa}, and specifically I_{Cap}, also makes a considerable contribution to an outward current, with an increase of $[Ca^{2+}]_i$ during the spike and in the subsequent repolarization (Fig. 7 *B*).

Note that similar APs can be obtained even in the absence of I_{KVs} if we substantially increase the current of I_{KCa}. For example, a fitting with $g_{KCa} = 70$ pS and $K_{KCa} = 0.3$ μM for I_{KCa} (at $I_{KVs} = 0$) leads to results similar to those shown in Figs. 6 *B* or 7 *B* (not shown). In this case, a slow increase in the K^+ outward current leading to a repolarization could be explained by an increase of I_{KCa} and I_{Cap} after the $[Ca^{2+}]_i$ increase during a single spike. Our model shows that if I_{VCa} is the depolarized current, then the repolarizing small currents, such as the resting current from I_{KDr} and some outward currents (I_{KVs} and/or I_{KCa} and I_{Cap}), which increase during a spike, can explain this complex oscillatory behavior.

Modeling the effects of TEA

Classical pharmacological blockers of voltage-gated K^+ channels such as TEA are often employed in β-cell electrophysiological studies despite a limited selectivity between different K^+ channels. The effects of TEA on K^+ channels were studied in cultured insulin-secreting HIT cells using

the patch-clamp technique (35). High TEA concentrations partially blocked the majority of islet K^+ channels, but it was a more effective inhibitor of TEA-sensitive K_{Ca} channels (EC_{50} = 0.15 mM) than of K_{ATP} channels (EC_{50} = 15 mM) or ''rapid'' delayed rectifier K^+ channels (EC_{50} = 3 mM) (35). However, the detailed mechanisms that lead to changes in spike behavior after TEA treatment remain unknown. We have modeled the action of TEA (15–20 mM of TEA is typically used in experiments) by decreasing the maximal conductance of K^+ currents (Figs. 6, *C* and *D*, and 7, *C* and *D*). We considered two hypothetical mechanisms.

In the first mechanism, we suggest that I_{KDr} and I_{KCa} were decreased almost entirely after TEA application, and no resting I_{KDr} current exists. Since I_{KATP} is less sensitive to TEA, the initial conductance of I_{KATP} was decreased by half (Figs. 6 *C* and 7 *C*). Fig. 7 *C* shows V_m, $[Ca^{2+}]_i$, and the various currents during simulation of one spike, as in Fig. 6 *C*. Activation of I_{VCa} depolarizes the membrane. Subsequently, the activation of TEA-insensitive I_{KVs} can contribute increasingly, leading to repolarization. This current has a small conductance in our model (5% of the whole-cell conductance of rapid delayed-rectifier K^+ channels), and its influence is observed only when I_{KDr} is inhibited and V_m increased. An increase in the I_{Cap} with $[Ca^{2+}]_i$ increase during a spike also plays a considerable part in the repolarization of the AP.

In the second mechanism, we simulated persistent activity of TEA-insensitive Ca^{2+}-dependent K^+ channels after TEA treatment (Fig. 6 *D*, and see Fig. 7 *D* for a single spike). The experimental basis for this proposal is the existence of some TEA-insensitive Ca^{2+}-dependent K^+ channels (see above and Discussion). However, the conductance and characteristics of this channel have not been adequately explored. As in the first mechanism, I_{KDr} was totally blocked. For simplicity, we also proposed that a slow voltage-activated K^+ outward current is absent in this case (I_{KVs} = 0). Thereafter, we attempted to determine the coefficients for the model that closely simulate AP behavior after TEA treatment. We found that when the conductance and half-maximal Ca^{2+} binding constant for I_{KCa} from Eqs. fdA16 and A17 were increased (from g_{mKCa} = 20 pS (Table 1) to g_{mKCa} = 200 pS and K_{KCa} from 0.1 μM (Table 1) to 0.3 μM), the simulation reproduced the characteristic AP after TEA application (Figs. 6 *D* and 7 *D*). The following mechanism is simulated in the model: when I_{KDr} and I_{KVs} were totally blocked, and conductivity of I_{KCa} was increased, an increase of $[Ca^{2+}]_i$ during a single spike leads to activation of I_{KCa} and I_{Cap}, with subsequent repolarization. The inclusion of this I_{KCa} conductance in our general model does not change the picture of simulated glucose-induced spikes represented in Fig. 5 or Fig. 7 *A* (not shown).

In both mechanisms, TEA simulation prolonged the AP and increased amplitude, but spike frequency was decreased (Fig. 6, *C* and *D*). This occurs because I_{KVs} (or I_{KCa} in the second mechanism) and I_{Cap} are smaller and activate more slowly compared with I_{KDr}. This allows I_{VCa} to progress to a point with higher V_m in the absence of I_{KDr} (Figs. 6, *C* and *D*, and 7, *C* and *D*). Nevertheless, in both cases, I_{KATP} makes also a contribution to outward K^+ currents with an increase of V_m, because the driving force of K^+ flux increases with a depolarization (Fig. 7, *C* and *D*, and see Eq. A13).

The two mechanisms generate spike patterns similar to what is seen in both $Kv2.1^{-/-}$ and control islets after TEA application (compare Fig. 6, *C* and *D*, with Figs. 3 *A3* and 4 *B2*, and with Fig. 2 from Jacobson et al. (14)). Our simulations are also consistent with previous observations (4,5,51,52). Thus, we can simulate the behavior of APs after TEA applications by almost entirely blocking the voltage-gated rapid delayed-rectifier K^+ channel conductance.

It is interesting to note that the TEA simulation at low (subthreshold) glucose ($[ADP]_i$ = 100 μM, see Table 2) does not lead to spike activity in our model. V_m was still lower (−43.25 mV) than the threshold level for spike generation (not shown). However, simulation of TEA effects diminishes the decrease in $[ADP]_i$ that is necessary for spike generation. In this case, spike generation takes place at $[ADP]_i$ = 50 μM instead of $[ADP]_i$ = 15 μM without a simulation of TEA action (not shown). This effect can be explained by blocking K_{ATP} channels with TEA that leads to decreased I_{KATP} even at moderate $[ADP]_i$ levels. These results agree with experimental data showing that TEA usually does not generate spikes at low glucose levels, but decreases the glucose level required for spike generation (4,51).

Burst activity and fast Ca^{2+} oscillations

AP bursts likely reflect slow periodic changes of some currents. This kind of change in overall current can lead to periodic repolarizations of plasma membrane potential (with a duration greater than several seconds) with similar $[Ca^{2+}]_i$ periodicity, usually described as $[Ca^{2+}]_i$ oscillations (see, e.g., Fig. 4 *A*, where one burst is represented, and (6,7,11,40)). The depolarizing component predominates at the beginning of the burst, but the resultant influx of Ca^{2+} during the burst may lead to a progressive increase in K^+ channel activity and/or a decrease in an inward Na^+ current, leading to repolarization (6,10,16,44). The model allows us to demonstrate that, for example, the cyclic simulation of the channel conductivity for K_{ATP} channels, Ca^{2+}-activated K^+ channels, and an inward Na^+ current can lead to a burst pattern in our model (Fig. 8, *A–E*) (for details, see Discussion). Note that in all cases only small changes in currents (in the range of 2 pA) were necessary to simulate burst behavior (see Fig. 8, *C–E*). Two or three of these current-activity changes may also act simultaneously during burst generation, requiring even smaller changes in the individual currents. The amplitude and frequency of APs progressively

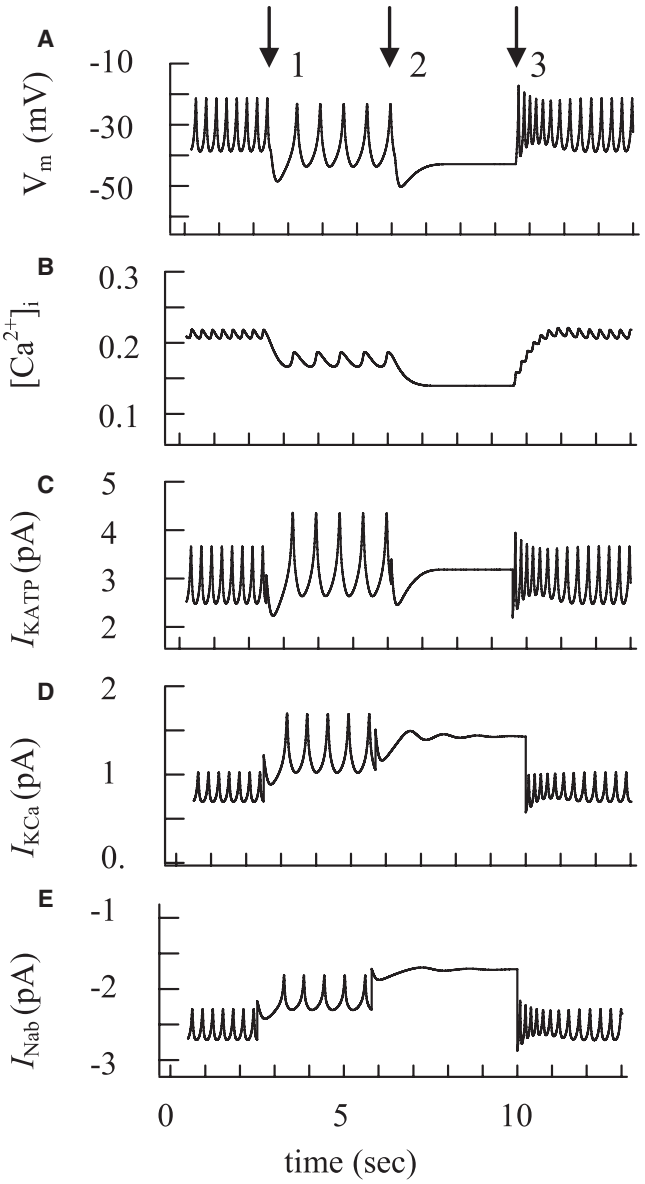

FIGURE 8 Simulation of glucose-induced burst activity and $[Ca^{2+}]_i$ with the initial simulation, as in Fig. 6 *A* for glucose-induced spikes in wild-type mouse. (*A–C*) Action potential (*A*), $[Ca^{2+}]_i$ (*B*), and I_{KATP} change (*C*) as regulators of bursting. Slow electrical bursting and $[Ca^{2+}]_i$ changes were simulated by a step increase and decrease of the K_{ATP} channel conductance by changes in $[ADP_f]_i$. At arrow 1, the $[ADP_f]_i$ was increased from 15 μM to 20 μM, at arrow 2 from 20 μM to 25 μM, and at arrow 3 from 25 μM back to 15 μM. (*D*) I_{KCa} change as a regulator of bursting. AP and $[Ca^{2+}]_i$ oscillations were simulated at a step increase and decrease of the K_{Ca} channel conductance. At arrow 1, the g_{mKCa} was increased from 20 pS to 35 pS, at arrow 2 from 35 pS to 50 pS, and at arrow 3 from 50 pS back to 20 pS. Only I_{KCa} is shown. AP and $[Ca^{2+}]_i$ changes were the same as in Fig. 8, *A* and *B*. (*E*) I_{Nab} change as a regulator of bursting. AP and $[Ca^{2+}]_i$ oscillations were simulated at a step decrease and increase of the Na^+ background current (I_{Nab}) conductance. At arrow 1, the g_{mNab} was decreased from 25 pS to 20 pS, at arrow 2 from 20 pS to 15 pS, and at arrow 3 from 15 pS back to 25 pS. Only I_{Nab} is shown. AP and $[Ca^{2+}]_i$ changes were the same as in Fig. 8, *A* and *B*.

decrease during the burst, terminated by repolarization and an electrically silent interval (see Fig. 4 *A*, for example, and (6,7,40)). This behavior was also simulated with a gradual cell repolarization in our model (Fig. 8 *A*).

DISCUSSION

We developed this model to gain further insights into coupling cation flux to $[Ca^{2+}]$ regulation in β-cells, a critical process for physiological insulin secretion that remains incompletely understood. We used the Hodgkin-Huxley formalism to describe the behavior of channels. This choice is consistent with our goal, to reconstruct the AP that results from ensemble currents through many individual channels. The key feature of the model is that it can be used to explore the putative mechanisms underlying AP spike activity. This semiquantitative model simulates the behavior of β-cell APs under a wide range of experimental conditions, including:

1. Changes in the period and amplitude of AP oscillations in response to glucose challenge.
2. Complex AP behavior due to K^+ channel blockade with TEA.
3. Increases in the duration of the plateau phase of AP spikes observed in response to specific $K_V2.1$ blockers.
4. Changes in islet electrical activity from the Kv2.1 null mouse compared with controls.

Chay and Keizer (9) described the first Hodgkin-Huxley-type ionic model based on electrophysiological data for β-cells, where generation of spikes was simulated as a result of an interaction between only two channels (voltage-gated Ca^{2+} and voltage-gated delayed-rectifier K^+ channels). Keizer and Magnus (10) improved this model by including K_{ATP} channels, an approach also used in later models to describe spikes in pancreatic β-cells (11,16). The temporal interaction of I_{VCa} and I_{KDr} is sufficient to explain the repetitive spiking observed in glucose-induced β-cells, simulating a reasonably accurate glucose-induced spike pattern (9,11,13). The interaction focusing on I_{VCa} and I_{KDr} was also used for a simulation of glucose-induced spikes in the model presented here. However, the use of mathematical models of APs where only the interaction between I_{VCa} and I_{KDr} is included presents difficulties for a detailed recapitulation of more complex experimental conditions. In particular, the spikes obtained from islets of Kv2.1 knockout mouse and the similar spikes obtained after application of specific Kv2.1 inhibitors (Fig. 3, *A2* and *B1*) had a specific complex shape that cannot readily be explained by existing models. These experimental results show that other channels must be included for an explanation of the regulation of spike activity in these circumstances. We found that implementing a small residual TEA-sensitive K_V current (I_{KDr}), TEA-insensitive slow-activated K^+ channels (I_{KVs}), or Ca^{2+}-activated K^+ current, as well as currents contributed by Ca^{2+} pumps, can help the model to more closely simulate the

full range of spike behavior observed experimentally, particularly in the absence of Kv2.1, or induced by application of TEA.

As in previous models, I_{VCa} is the major depolarizing current during spike generation. For the I_{KDr} conductance, our simulations show that Kv2.1 is a likely candidate for the principal delayed-rectifier isoform expressed in mouse β-cells, in keeping with findings from several experimental studies (14,32). The absence of Kv2.1 channels results in an increased glucose-stimulated AP duration, a decreased firing frequency, and a complex AP behavior (Fig. 3, *A2* and *B1*; see also Jacobson et al. (14)). These changes in AP can be explained by the existence of other K_v currents (I_{KCa}, I_{KVs}, and residual I_{KDr} current, which remain intact after blockade of Kv2.1 channels) and I_{Cap} (see Figs. 6 *B* and 7 *B*). By reducing the I_{KDr} conductance 10-fold in the model, the simulated complex spikes resembled the spike picture in experiments with Kv2.1$^{-/-}$ islets. However, in contrast to mouse, the Kv2.1 isoform appears to make only a small contribution in human β-cells, consistent with observations that Kv2.1 blockade had only modest effects on electrical activity (33).

Which channels can be responsible for these currents?

Residual I_{KDr} current, which remains intact after blockade of Kv2.1 channels

According to our simulations to explain the complex behavior of APs obtained after elimination of Kv2.1 channels, the conductance I_{KDr} should be reduced to ~10% of the initial I_{KDr} conductance to obtain a residual current that has detectable effect. Such a small residual TEA-dependent K_V current is indeed detectable in the Kv2.1 null mouse islets (14). However, it remains incompletely characterized. There is limited data on molecular identification of all of the non-Kv2.1 channels involved in the TEA-sensitive part of the K_V current. Some channels other than Kv2.1 channels expressed in β-cells are TEA-sensitive, for example, Kv3.1 and Kv3.2 (36,53) and could be responsible for the residual TEA-sensitive K_V current.

Small TEA-insensitive voltage-dependent current (I_{KVs})

We set the conductance for this current to 5% of the total K_V channel conductance (see Table 1) and found that this small value is enough to closely approximate experimental data. A small TEA-insensitive current really found in β-cells contributes to the outward K^+ current, and its maximal conductance is within the range used in our model for I_{KVs} (34–36,54). However, to accurately describe the experimental data, in particular the prolongation of AP duration with TEA, our model used a slow activation time (300 ms in Table 1) for this current.

Which TEA-insensitive channels can lead to repolarization during a spike after TEA application, and what other characteristics should it display? We can rule out residual TEA-sensitive Kv2.1 channels, because spike behavior after TEA application is similar in wild-type and K_V2.1 knockout mouse islets (see Fig. 3, *A3* and *B2*). TEA-insensitive Kv1.4 and/or Kv4.2 channels could contribute to an inactivating portion of MIN6 cell outward K^+ current recorded after TEA application (54). Another candidate is the TEA-insensitive voltage-gated KCNQ1 channel that was detected in INS-1 cells and in mouse islets (55). The TEA-insensitive voltage-gated ether-a-go-go K^+ channels (or human ERG channels) can also influence both insulin secretion and AP firing frequency in isolated human islets (56). ERG channels were found recently in β-cells from rat islets (57). Interestingly, ERG currents activate slowly (in several seconds) upon depolarization to potentials below 0 mV (58). This time-activated kinetics of the ERG current looks remarkably similar to the proposed I_{KVs} current in our model.

We also found that the spike shape in β-cells after blockade of Kv channel by TEA resembles the AP in the cardiac sinoatrial node myocytes (see, e.g., Berecki et al. (59)). In these cells a fast Na^+ current appears to be small or absent (60) and the AP activating mechanisms may be determined by Ca^{2+} and K_V channels interacting, similar to the spike generating mechanism in β-cells. The slow- as well as fast-activating delayed-rectifier K^+ channels were found in cardiac sinoatrial node myocytes. In these cells, the slow-activating K^+ channels are activated at membrane potentials similar to those for fast-activating K^+ channels but with different kinetics, and these slowly-activated currents determine the latter phase of repolarization (20). HERG and KCNQ1 K^+ channels play a major role in action potential repolarization in these myocytes (59,60). Based on these investigations, we can suggest that TEA-insensitive voltage-dependent KCNQ1 and/or HERG channels could contribute to the slowly-activated voltage-gated K^+ channels in β-cells. However, further studies are needed to better understand these channels in β-cells from different species.

Plasma membrane Ca^{2+}-pump current (I_{Cap}) and Ca^{2+}-activated K^+ current (I_{KCa})

We investigated another possible explanation for spike generation in cases where APs are long and of high amplitude. The relative Ca^{2+} concentration increases moderately during each glucose-generated spike (Fig. 4 *A*) in comparison with Ca^{2+} changes during high amplitude with slow spikes after Kv2.1 channel blockade (see Fig. 4 in Jacobson et al. (14)) or TEA application (Fig. 4 *B*). Other studies using Ca^{2+}-sensing fluorescent dyes to monitor temporal changes have also shown small but detectable changes in $[Ca^{2+}]_i$ within tens of milliseconds during a single glucose-induced electrical spike followed by large-amplitude $[Ca^{2+}]_i$ changes after TEA application (52).

As the $[Ca^{2+}]_i$ oscillations are small, the changes in Ca^{2+}-dependent currents (I_{KCa} and I_{Cap}) are also small compared

with the change of I_{KDr} during the simulation of glucose-generated spikes in wild-type mouse islets (see Figs. 6 *A* and 7 *A*) and provide only background currents in our model. However, the larger $[Ca^{2+}]_i$ increase during single TEA or Kv2.1 block-induced spikes can activate I_{KCa} and I_{Cap} (Fig. 7, *C* and *D*). In this case, TEA-insensitive small-conductance voltage-independent, Ca^{2+}-dependent K^+ channels and I_{Cap} could contribute to repolarization of APs and, together with I_{VCa}, could also be considered as candidate pacemakers for some long and high-amplitude spikes.

Spike repolarization induced by I_{KCa} activation was originally suggested in earlier studies (12,61). However, a role for I_{Cap} was not considered. Surprisingly, the results of the simulations show that a plasma membrane Ca^{2+}-pump current can also contribute to the AP mechanism when spikes have high amplitude and low frequency.

Which Ca^{2+}-activated K^+ channels can be responsible for repolarization during a spike after TEA application or after Kv2.1 channel blockade? Several Ca^{2+}-activated K^+ channels are expressed in β-cells. One of them is highly TEA-sensitive (Kd <1 mM), the maxi-K_{Ca} (BK_{Ca}, slo)-like channels (18,62). Another class of K_{Ca} channel genes expressed in β-cells is the small-conductance (SK) channels (18,41). Small-conductance K_{Ca} channels, in particular SK4, are only weakly sensitive to TEA (63). These channels could be responsible for a TEA-insensitive voltage-independent Ca^{2+}-dependent current in our model.

Note that our model suggests that the mechanism for specific amplification of spike activity leads to increased $[Ca^{2+}]_i$, which correspondingly may enhance glucose-dependent insulin secretion, similar to the results with blockers of the β-cell K_{ATP} channels (Figs. 5 and 6). If useful tissue specificity could be engineered, such blockers might provide alternatives to currently available treatment for type 2 diabetes (3,32,64).

Bursts of APs and the Ca^{2+} oscillations

Mechanisms that generate and terminate spikes are responsible for the bursts of APs and Ca^{2+} oscillations. Changes in voltage-gated Ca^{2+} and K^+ currents and/or voltage-independent gating variable currents can take part in burst generation. For example, the spikes and the burst itself can be terminated during a single burst, if some parameters in the equations for voltage-gated currents (for example, I_{VCa}, I_{KDr}, and I_{KVs} in our model) that we accepted as constants can instead change slowly in comparison with a single spike period. This would require drift in a direction leading to V_m repolarization and spike and burst cancellation. Such a mechanism may require modeling of time-dependent changes of coefficients in the equations for voltage-gated currents. However, at this time, there is no experimental evidence for this kind of mechanism. Another hypothesis concerning the mechanisms of spike generation and cancellation during the bursts employs slow cyclic changes in conductance of the voltage-independent gating variable currents. For example:

1. A $[Ca^{2+}]_i$ increase during a burst can lead to a decrease in ATP/ADP ratio, leading to opening of K_{ATP} channels and plasma membrane depolarization (8,10,16). We found that repolarization followed by a silent interval with a $[Ca^{2+}]_i$ decrease can be simulated by a gradual increase of K_{ATP} channel conductance after an increase in free [ADP] to 5 μM and 10 μM, correspondingly. Decreasing ADP concentration to initial levels restored spike activity and generated the burst (Fig. 8, *A–C*).
2. An increase in K^+ channel activity can occur via an effect on slowly-activating and deactivated specific Ca^{2+}-activated K^+ channels (6,37). This channel was not directly modeled here. However, we were able to reproduce the reversible conductivity changes in Ca^{2+}-activated K^+ channels in general. Fig. 8 *D* shows the burst behavior that can be simulated by an increase and a decrease of I_{KCa} conductance. (Note that in the second and third cases, the behavior of APs and $[Ca^{2+}]_i$ was the same as for the first mechanism, and we do not show them separately.)
3. Increased $[Ca^{2+}]_i$ can lead to increased $[Ca^{2+}]$ in endoplasmic reticulum. This decreases an inward Na^+ or Ca^{2+} current through nonselective cation channels (16,44,45). We simulated this mechanism by gradually decreasing I_{Nab} conductance, with a subsequent increase (Fig. 8 *E*). It also leads to a simulation of the burst and the corresponding Ca^{2+} changes.

Our simulations in Fig. 8 show clearly that after the large depolarizing effect of closing K_{ATP} channels, the subsequent generation and termination of the bursts can be determined by small cyclic changes, in the range of 2 pA, of the background voltage-independent gating variable currents. Several suggestions have been made as to the mechanism that underlies the cyclic changes in the conductivity of some background currents (further discussion can be found in (11,16,17,65)).

CONCLUSION

Our experiments on Kv2.1$^{-/-}$ mouse islet cells, using specific Kv2.1 channel inhibitors and TEA application with model simulations, demonstrate the importance of Kv2.1 channels and also implicate other K_V channels in AP regulation. This suggests that other voltage-gated K^+ channels, along with Kv2.1 channels, not only take part in regulating normal spike activity but are able to control spikes in the membrane potential in the absence of Kv2.1 channels. It was possible to achieve a reasonable fit between our experimental results and a general mathematical model by employing a voltage-gated calcium current, a delayed-rectifier K^+ current, a small slowly-activating K^+ current, and several voltage-gated independent K^+ and Na^+ background currents. The results of the computer simulations using this adaptable model of islet AP spikes provide insight into the mechanism by which each channel contributes to APs under a variety of experimental conditions.

APPENDIX: MODEL EQUATIONS AND PARAMETERS

Ca^{2+} current (I_{VCa})

$$I_{VCa} = g_{mVCa} d_{Ca} f_{VCa} f_{2Ca} (V_m - E_{Ca}) \quad (A1)$$

$$\frac{d\, d_{Ca}}{dt} = \frac{d_{Ca\infty} - d_{Ca}}{\tau_{dCa}} \quad (A2)$$

$$d_{Ca\infty} = 0.002 + \frac{1}{1 + \exp[(-2 - V_m)/8.8]} \quad (A3)$$

$$\tau_{dCa} = 2.2 - 1.79 * \exp - [(V_m - 9.7)/70.2]^2 \quad (A4)$$

$$f_{VCa} = f_{VCa\infty} = \frac{1}{1 + \exp[(9 + V_m)/8]} \quad (A5)$$

$$\frac{df_{2Ca}}{dt} = 0.007(1 - f_{2Ca}) - 0.0025(-I_{VCa}/g_{mVCa}) f_{2Ca} \quad (A6)$$

Delayed rectifier K^+ current (I_{KDr})

$$I_{KDr} = g_{mKDr}\, d_{KDr}^2 f_{KDr} (V_m - E_K), \quad (A7)$$

$$\frac{d\, d_{KDr}}{dt} = \frac{d_{KDr} - d_{KDr}}{t_{dKDr\infty}} \quad (A8)$$

$$d_{KDr\infty} = \frac{1}{1 + \exp[(-9 - V_m)/5]} \quad (A9)$$

Slow-activated TEA-insensitive K^+ current (I_{KVs})

$$I_{KVs} = g_{mKVs}\, d_{Ks}^2 f_{KDr} (V_m - E_K), \quad (A10)$$

$$\frac{dd_{Ks}}{dt} = \frac{d_{Ks} - d_{Ks}}{\tau_{dKs\infty}} \quad (A11)$$

$$d_{Ks\infty} = \frac{1}{1 + \exp[(-9 - V_m)/5]} \quad (A12)$$

ATP-sensitive K^+ channel current (I_{KATP})

$$I_{KATP} = g_{mKATP} O_{KATP} (V_m - E_K), \quad (A13)$$

where

$$O_{KATP} = \frac{0.08\left(1 + 2\left[MgADP_f\right]_i/17\right) + 0.89\left(\left[MgADP_f\right]_i/17\right)^2}{\left(1 + \left[MgADP_f\right]_i/17\right)^2 \left(1 + 0.45\left[MgADP_f\right]_i/26 + \left[ATP_{free}\right]_i/50\right)} \quad (A14)$$

$$\left[MgADP_f\right]_i = 0.55\left[ADP_f\right]_i, \quad (A15)$$

where O_{KATP} is the fraction of open K_{ATP} channels, $MgADP_f$ is free Mg-bound ADP, $[ADP_f]_i$ is free ADP concentration in cytoplasm.

Ca^{2+}-activated K^+ current (I_{KCa})

$$I_{KCa} = g_{mKCa} f_{KCa} (V_m - E_K), \quad (A16)$$

where

$$f_{KCa} = \frac{\left[Ca^{2+}\right]_i^4}{\left[Ca^{2+}\right]_i^4 + K_{KCa}^4}. \quad (A17)$$

Plasma membrane Ca^{2+} pump current (I_{Cap})

$$I_{Cap} = P_{mCap} \frac{\left[Ca^{2+}\right]_i^2}{\left[Ca^{2+}\right]_i^2 + K_{Cap}^2}. \quad (A18)$$

Na^+ background current (I_{Nab})

$$I_{Nab} = g_{mNab} (V_m - E_{Na}). \quad (A19)$$

We thank N. Tamarina for helpful discussions. This work was supported by National Institutes of Health grant DK48494 (L.H.P.) and University of Chicago grants DRTC P60 and DK20595.

REFERENCES

1. Ashcroft, F. M., and P. Rorsman. 1989. Electrophysiology of the pancreatic β-cell. *Prog. Biophys. Mol. Biol.* 54:87–143.
2. Houamed, K., J. Fu, M. W. Roe, and L. H. Philipson. 2004. Electrophysiology of the pancreatic β cell. *In* Diabetes Mellitus: A Fundamental and Clinical Text, 3rd ed. D. LeRoith, S. I. Taylor, and J. O. Olefsky, editors. Lippincott, Williams and Wilkins, Philadelphia. 51–68.

3. Jacobson, D. A., and L. H. Philipson. 2007. Action potentials and insulin secretion: new insights into the role of Kv channels. *Diabetes Obes. Metab.* 9 (Suppl 2):89–98.
4. Atwater, I., B. Ribalet, and E. Rojas. 1979. Mouse pancreatic β-cells: tetrathylammonium blockage of the potassium permeability increase induced by depolarization. *J. Physiol.* 288:561–574.
5. Lebrun, P., and I. Atwater. 1985. Effects of the calcium channel agonist, BAY K 8644, on electrical activity in mouse pancreatic β-cells. *Biophys. J.* 48:919–930.
6. Göpel, S. O., T. Kanno, S. Barg, L. Eliasson, J. Galvanovskis, et al. 1999. Activation of Ca^{2+}-dependent K^+ channels contributes to rhythmic firing of action potentials in mouse pancreatic β-cells. *J. Gen. Physiol.* 114:759–770.
7. Antunes, C. M., A. P. Salgado, L. M. Rosario, and R. M. Santos. 2000. Differential patterns of glucose-induced electrical activity and intracellular calcium responses in single mouse and rat pancreatic islets. *Diabetes.* 49:2028–2038.
8. Kanno, T., P. Rorsman, and S. O. Gopel. 2002. Glucose-dependent regulation of rhythmic action potential firing in pancreatic β-cells by K_{ATP}-channel modulation. *J. Physiol.* 545:501–507.
9. Chay, T. R., and J. Keizer. 1983. Minimal model for membrane oscillations in the pancreatic β-cell. *Biophys. J.* 42:181–190.
10. Keizer, J., and G. Magnus. 1989. ATP-sensitive potassium channel and bursting in the pancreatic beta cell. A theoretical study. *Biophys. J.* 56:229–242.
11. Sherman, A. 1996. Contributions of modeling to understanding stimulus-secretion coupling in pancreatic β-cells. *Am. J. Physiol. Endocrinol. Metab.* 271:E362–E372.
12. Chay, T. R. 1997. Effects of extracellular calcium on electrical bursting and intracellular and luminal calcium oscillations in insulin secreting pancreatic β-cells. *Biophys. J.* 73:1673–1688.
13. Tamarina, N. A., A. Kuznetsov, L. E. Fridlyand, and L. H. Philipson. 2005. Delayed-rectifier (KV2.1) regulation of pancreatic β-cell calcium responses to glucose: inhibitor specificity and modeling. *Am. J. Physiol. Endocrinol. Metab.* 289:E578–E585.
14. Jacobson, D. A., A. Kuznetsov, J. P. Lopez, S. Kash, C. E. Ämmälä, et al. 2007. Kv2.1 Ablation alters glucose induced islet electrical activity. Enhancing insulin secretion. *Cell Metab.* 6:229–235.
15. Bao, S., D. A. Jacobson, M. Wohltmann, A. Bohrer, W. Jin, et al. 2008. Glucose homeostasis, insulin secretion, and islet phospholipids in mice that overexpress iPLA2β in pancreatic. β-cells and in iPLA2β-null mice. *Am. J. Physiol. Endocrinol. Metab.* 294:E217–E229.
16. Fridlyand, L. E., N. Tamarina, and L. H. Philipson. 2003. Modeling of Ca^{2+} flux in pancreatic β-cells: role of the plasma membrane and intracellular stores. *Am. J. Physiol. Endocrinol. Metab.* 285:E138–E154.
17. Fridlyand, L. E., L. Ma, and L. H. Philipson. 2005. Adenine nucleotide regulation in pancreatic β-cells: modeling of ATP/ADP-Ca^{2+} interactions. *Am. J. Physiol. Endocrinol. Metab.* 289:E839–E848.
18. Yang, S. N., and P. O. Berggren. 2005. β-cell CaV channel regulation in physiology and pathophysiology. *Am. J. Physiol. Endocrinol. Metab.* 288:E16–E28.
19. Mears, D., and E. Rojas. 2006. Properties of voltage-gated Ca^{2+} currents measured from mouse pancreatic β-cells in situ. *Biol. Res.* 39:505–520.
20. Nerbonne, J. M., and R. S. Kass. 2005. Molecular physiology of cardiac repolarization. *Physiol. Rev.* 85:1205–1253.
21. Cens, T., M. Rousset, J. P. Leyris, P. Fesquet, and P. Charnet. 2006. Voltage- and calcium-dependent inactivation in high voltage-gated Ca^{2+} channels. *Prog. Biophys. Mol. Biol.* 90:104–117.
22. Plant, T. D. 1988. Properties and calcium-dependent inactivation of calcium currents in cultured mouse pancreatic β-cells. *J. Physiol.* 404:731–747.
23. Satin, L. S., and D. L. Cook. 1989. Calcium current inactivation in insulin-secreting cells is mediated by calcium influx and membrane depolarization. *Pflugers Arch.* 414:1–10.
24. Göpel, S. O., T. Kanno, S. Barg, L. Eliasson, J. Galvanovskis, et al. 1999. Voltage-gated and resting membrane currents recorded from β-cells in intact mouse pancreatic islets. *J. Physiol.* 21:717–728.
25. DiFrancesco, D., and D. Noble. 1985. A model of cardiac electrical activity incorporating ionic pumps and concentration changes. *Philos. Trans. R. Soc. Lond. B Biol. Sci.* 307:353–398.
26. Luo, C. H., and Y. Rudy. 1994. A dynamic model of the cardiac ventricular action potential. I. Simulations of ionic currents and concentration changes. *Circ. Res.* 74:1071–1096.
27. Bondarenko, V. E., G. C. Bett, and R. L. Rasmusson. 2004. A model of graded calcium release and L-type Ca^{2+} channel inactivation in cardiac muscle. *Am. J. Physiol. Heart Circ. Physiol.* 286:H1154–H1169.
28. Rorsman, P., and G. Trube. 1986. Calcium and delayed potassium currents in mouse pancreatic β-cells under voltage-clamp conditions. *J. Physiol.* 374:531–550.
29. Bokvist, K., C. Ammala, P. O. Berggren, P. Rorsman, and K. Wahlander. 1991. α2-adrenoreceptor stimulation does not inhibit L-type calcium channels in mouse pancreatic β-cells. *Biosci. Rep.* 11:147–157.
30. Sherman, A., J. Keizer, and J. Rinzel. 1990. Domain model for Ca^{2+}-inactivation of Ca^{2+} channels at low channel density. *Biophys. J.* 58: 985–995.
31. Smith, P. A., K. Bokvist, P. Arkhammar, P.-O. Berggren, and P. Rorsman. 1990. Delayed rectifying and calcium-activated K^+ channels and their significance for action potential repolarization in mouse pancreatic *Biophys. J* -cells. *J. Gen. Physiol.* 95:1041–1059.
32. MacDonald, P. E., X. F. Ha, J. Wang, S. R. Smukler, A. M. Sun, et al. 2002. Members of the Kv1 and Kv2 voltage-dependent K^+ channel families regulate insulin secretion. *Mol. Endocrinol.* 15:1423–1435.
33. Braun, M., R. Ramracheya, M. Bengtsson, Q. Zhang, J. Karanauskaite, et al. 2008. Voltage-gated ion channels in human pancreatic β-cells. Electrophysiological characterization and role in insulin secretion. *Diabetes.* 57:1618–1628.
34. Bokvist, K., P. Rorsman, and P. A. Smith. 1990. Effects of external tetraethylammonium ions and quinine on delayed rectifying K^+ channels in mouse pancreatic β-cells. *J. Physiol.* 423:311–325.
35. Fatherazi, S., and D. L. Cook. 1991. Specificity of tetraethylammonium and quinine for three K^+ channels in insulin-secreting cells. *J. Membr. Biol.* 120:105–114.
36. Su, J., H. Yu, N. Lenka, J. Hescheler, and S. Ullrich. 2001. The expression and regulation of depolarization-activated K^+ channels in the insulin-secreting cell line INS-1. *Pflugers Arch.* 442:49–56.
37. Zhang, M., K. Houamed, S. Kupershmidt, D. Roden, and L. S. Satin. 2005. Pharmacological properties and functional role of K_{slow} current in mouse pancreatic β-cells: SK channels contribute to K_{slow} tail current and modulate insulin secretion. *J. Gen. Physiol.* 126:353–363.
38. Rorsman, P., and G. Trube. 1985. Glucose dependent K^+-channels in pancreatic β-cells are regulated by intracellular ATP. *Pflugers Arch.* 405:305–309.
39. Misler, S., W. M. Gee, K. D. Gillis, D. W. Scharp, and L. C. Falke. 1989. Metabolite-regulated ATP-sensitive K^+ channel in human pancreatic islet cells. *Diabetes.* 38:422–427.
40. Kinard, T. A., G. de Vries, A. Sherman, and L. S. Satin. 1999. Modulation of the bursting properties of single mouse pancreatic β-cells by artificial conductances. *Biophys. J.* 76:1423–1435.
41. Tamarina, N. A., Y. Wang, L. Mariotto, A. Kuznetsov, C. Bond, et al. 2003. Small-conductance calcium-activated K^+ channels are expressed in pancreatic islets and regulate glucose responses. *Diabetes.* 52:2000–2006.
42. Kozak, J. A., S. Misler, and D. E. Logothetis. 1998. Characterization of a Ca^{2+}-activated K^+ current in insulin-secreting murine βTC-3 cells. *J. Physiol.* 509:355–370.
43. Hao, L., J.-L. Rigaud, and G. Inesi. 1994. Ca^{2+}/H^+ countertransport and electrogenicity in proteoliposomes containing erythrocyte plasma membrane Ca-ATPase and exogenous lipids. *J. Biol. Chem.* 269: 14268–14275.
44. Bertram, R., P. Smolen, A. Sherman, D. Mears, I. Atwater, et al. 1995. A role for calcium release-activated current (CRAC) in cholinergic

modulation of electrical activity in pancreatic β-cells. *Biophys. J.* 68: 2323–2332.

45. Roe, M. W., J. F. Worley 3rd, F. Qian, N. Tamarina, A. A. Mittal, et al. 1998. Characterization of a Ca^{2+} release-activated nonselective cation current regulating membrane potential and Ca^{2+} oscillations in transgenically derived β-cells. *J. Biol. Chem.* 273:10402–10410.
46. Leech, C. A., and J. F. Habener. 1998. A role for Ca^{2+} sensitive nonselective cation channels in regulating the membrane potential of pancreatic β-cells. *Diabetes.* 47:1066–1073.
47. Jacobson, D. A., and L. H. Philipson. 2007. TRP channels of the pancreatic β cell. *Handb. Exp. Pharmacol.* 179:409–424.
48. Kelly, R. P., R. Sutton, and F. M. Ashcroft. 1991. Voltage-activated calcium and potassium currents in human pancreatic β-cells. *J. Physiol.* 443:175–192.
49. Pressel, D. M., and S. Misler. 1990. Sodium channels contribute to action potential generation in canine and human pancreatic islet β-cells. *J. Membr. Biol.* 116:273–280.
50. Reference deleted in proof.
51. Henquin, J. C. 1990. Role of voltage- and Ca^{2+} dependent K^+ channels in the control of glucose-induced electrical activity in pancreatic β-cells. *Pflugers Arch.* 416:568–572.
52. Santos, R. M., L. M. Rosario, A. Nadal, J. Garcia-Sancho, B. Soria, et al. 1991. Widespread synchronous Ca^{2+} oscillations due to bursting electrical activity in single pancreatic islets. *Eur. J. Phys.* 418:417–422.
53. Dukes, I. D., and L. H. Philipson. 1996. K^+ channels: generating excitement in pancreatic β-cells. *Diabetes.* 45:845–853.
54. MacDonald, P. E., S. Sewing, J. Wang, J. W. Joseph, S. R. Smukler, et al. 2002. Inhibition of Kv2.1 voltage-dependent K^+ channels in pancreatic β-cells enhances glucose-dependent insulin secretion. *J. Biol. Chem.* 22:44938–44945.
55. Ullrich, S., J. Su, F. Ranta, O. H. Wittekindt, F. Ris, et al. 2005. Effects of I(Ks) channel inhibitors in insulin-secreting INS-1 cells. *Pflugers Arch.* 451:428–436.
56. Rosati, B., P. Marchetti, O. Crociani, M. Lecchi, R. Lupi, et al. 2000. Glucose- and arginine-induced insulin secretion by human pancreatic β-cells: the role of HERG K^+ channels in firing and release. *FASEB J.* 14:2601–2610.
57. Mühlbauer, E., I. Bazwinsky, S. Wolgast, A. Klemenz, and E. Peschke. 2007. Circadian changes of ether-a-go-go-related-gene (Erg) potassium channel transcripts in the rat pancreas and β-cell. *Cell. Mol. Life Sci.* 64:768–780.
58. Schwarz, J. R., and C. K. Bauer. 2004. Functions of erg K^+ channels in excitable cells. *J. Cell. Mol. Med.* 8:22–30.
59. Berecki, G., J. G. Zegers, A. O. Verkerk, Z. A. Bhuiyan, B. de Jonge, et al. 2005. HERG channel (dys)function revealed by dynamic action potential clamp technique. *Biophys. J.* 88:566–578.
60. Rudy, Y., and J. R. Silva. 2006. Computational biology in the study of cardiac ion channels and cell electrophysiology. *Q. Rev. Biophys.* 39:57–116.
61. Velasco, J. M., and O. H. Petersen. 1987. Voltage-activation of high-conductance K^+ channel in the insulin-secreting cell line RINm5F is dependent on local extracellular Ca^{2+} concentration. *Biochim. Biophys. Acta.* 896:305–310.
62. Tabcharani, J. A., and S. Misler. 1989. Ca^{2+}-activated K^+ channel in rat pancreatic islet β cells: permeation, gating and blockade by cations. *Biochim. Biophys. Acta.* 982:62–72.
63. Joiner, W. J., L. Y. Wang, M. D. Tang, and L. K. Kaczmarek. 1997. hSK4, a member of a novel subfamily of calcium-activated potassium channels. *Proc. Natl. Acad. Sci. USA.* 94:11013–11018.
64. Herrington, J., Y.-P. Zhou, R. M. Bugianesi, P. M. Dulski, Y. Feng, et al. 2006. Blockers of the delayed-rectifier potassium current in pancreatic β-cells enhance glucose-dependent insulin secretion. *Diabetes.* 55:1034–1042.
65. Bertram, R., A. Sherman, and L. S. Satin. 2007. Metabolic and electrical oscillations: partners in controlling pulsatile insulin secretion. *Am. J. Physiol. Endocrinol. Metab.* 293:E890–E900.